M G CARVALHO PhD,* P OLIVEIRA MSc† and V SEMIAO MSc*

A three-dimensional modelling of an industrial glass furnace

A mathematical model for the prediction of the performance of an industrial glass furnace is described. It comprises sub-models for the combustion chamber and the glass tank flow. The first sub-model incorporates physical modelling for the turbulent diffusion flame, soot formation and consumption and the thermal radiation. The SIMPLE algorithm is used here to solve the finite-difference equations derived from the partial non-linear differential equations of the mathematical model. The second sub-model incorporates physical modelling for the laminar flow and energy balance of the molten glass, driven by free convection. The PISO algorithm is used in this sub-model to solve the finite-difference equations. The whole mathematical model is applied to a cross-fired regenerative furnace. An iterative procedure is used, where the heat transfer to the upper surface of the molten glass is that calculated for the combustion chamber, by the first sub-model, assuming known values of the temperatures of the referred surface. These temperatures are calculated by the second sub-model using as boundary condition the heat transfer fluxes calculated by the first sub-model. The whole procedure is repeated until 'convergence' is achieved. The results have shown a strong dependence between the physical processes occurring in the combustion chamber and in the glass tank and therefore, unless a set of reliable data of temperature of the glass surface is available, the prediction for this kind of furnace should include the glass tank

1. List of symbols

A_p, a_p	finite-difference equation coefficient for point P
a_n	finite-difference equation coefficient for the neighbour points (N, S, E, W, U, D) of P
C_{pj}	constant pressure specific heat of species j
E	activation energy
	black body emissive power
f	mixture fraction
g	variance of mixture fraction
g_i	gravitational acceleration in the i-direction
$\tilde{h}$	time-mean stagnation enthalpy
I	intensity of radiant energy
k_i	absorption coefficients of the i species
K_{eff}	effective thermal conductivity of the glass
k	turbulent kinetic energy
L	path length
l	local length scale of turbulence
M_j	molecular weight of the species j
m_j	time-averaged mass concentration of species j
$P(f)$	'normal' probability density function
p	pressure
q_P	flux at a point P on a wall boundary
R	universal gas constant
S_P, S_o	source-term of the finite-difference equations
s_j	stoichiometric oxygen requirement of unit mass of a species j
T	temperature
u_i	velocity component in the i-direction

Greek symbols

β	volumetric coefficient of thermal expansion
Γ_ϕ	molecular exchange coefficient for a variable ϕ
Δ_i	discretised divergence
δ_{ij}	Kronecker's delta
ε	dissipation rate of turbulent energy
	total emittance
ε_w	emissivity of wall
μ	molecular viscosity
μ_{eff}	effective viscosity
μ_t	turbulent viscosity
ρ	time-mean density
σ_ϕ	Prandtl number for a variable ϕ
ϕ	surrogate variable f, g, $\tilde{h}$, k, ε and m_s
	single passive scalar, eqn (11)
	equivalence ratio, eqn (19(a))
Ω	solid angle

Superscripts

*	guessed value
'	fluctuation component
—	time-averaged value
n	number of iteration
**	first corrector stage for velocity
	second corrector stage for pressure
***	second corrector stage for velocity

Subscripts

fu	fuel
g	gas
in	inlet
ox	oxidant
s	soot
w	wall

2. Introduction

2.1. Preamble

The recent awareness of the limitation of energy resources, the increase in fuel prices, and the problem of pollution have turned combustion engineers' attention towards the importance of improving combustion equipment design.

Increasing pressure is being placed on engineers to have recourse to every available modern theoretical and analytical means to quantify and enhance the industrial furnace performance criteria. There is currently considerable interest from the glass and ceramics industry to support the construction of a mathematical model which reliably simulates the performance of the glass melting furnaces. Glass furnaces are large and so they are extremely costly to develop by highly empirical methods.

Most of the previous glass furnace predictive studies have avoided the complexities of the combustion chamber region and confined attention to the flow in the tank, see refs 1, 2 and 3, for example.

*Instituto Superior Tecnico, University of Lisbon, Department of Mechanical Engineering, Lisbon, Portugal.
†Imperial College of Science and Technology, Department of Mineral Resources Engineering, London; formerly Instituto Superior Tecnico, University of Lisbon.

combustion chamber in which the flow field and heat release were determined from a numerical solution of the governing balance equations was presented by Gosman *et al.*[4] The works of Carvalho[5] and Semiao[6] have extended this simulation to more complex geometries with a horseshoe-flow shape. The predictions of Semiao[6] were made to oxygen-rich burning conditions. The work of Carvalho, Durão and Pereira[7] is an extension of Semiao's work[6] in which the authors have used a two-dimensional axisymmetric model to simulate the burner region, providing with these results the inlet conditions for the three-dimensional calculations of the combustion chamber. The results were extensively validated with experimental data acquired in the furnace used in work by Carvalho *et al.*[8]

There have been very few attempts to model a complete glass furnace. A simplified model was presented by McConnell and Goodson[9] in which global energy equations for the combustion chamber, molten glass and feed ('batch') were solved for an assumed flow and heat release, Hottel's zone method being used to calculate the combustion chamber radiation. A similar study was effected by Mase and Oda,[10] but the flow field in the molten glass was solved assuming two-dimensionality. A further study of this kind has been carried out by Novak,[11] in which the combustion chamber flow field was more carefully estimated with the assistance of empirical data for non-reacting flows for cylindrical ducts. The investigation of Carvalho and Lockwood[12] extended the work presented by Carvalho[5] and brought into analysis the batch and glass tank flows, assuming two-dimensionality of the batch flow. The glass tank flow predictions were made with a three-dimensional computer procedure.

The present work deals with a completely three-dimensional simulation of an industrial glass furnace, in which a new elaborated model to predict the glass tank flow was used.

The combustion chamber and the molten glass flow were studied by a cyclical iterative way, by separated calculations. Assuming known values of the temperature of the glass surface, the flow, combustion process and heat fluxes in the combustion chamber were predicted by a three-dimensional solution technique, which forms the first sub-model. Using the calculated heat flux to the glass surface as a boundary condition, the flow and the temperature distribution in the molten glass were predicted by a different three-dimensional numerical technique, which forms the second sub-model. These glass surface temperatures were then introduced as a boundary condition in the first sub-model framing a cyclical iterative procedure; that 'converged' solution allows one to predict the performance of the whole furnace. In the second sub-model, a non-iterative method of handling the pressure/velocity coupling that arises in the implicitly discretised fluid flow equations (PISO[13]) was used. The use of PISO results in a substantial reduction in computing effort over that required by iterative methods.[14]

This paper contains six sections: section 2 forms the introduction; section 3 is devoted to physical modelling and section 4 describes the essential features of the computer method for solving the complete set of equations. The application of the numerical procedure to a large industrial furnace, the presentation and discussion of the results are included in section 5. Concluding remarks are presented in section 6.

2.2 Description of furnace

Fig. 1 shows a sketch of the furnace, which is of the cross-fired regenerative kind. The furnace is essentially a large insulated container in which the batch enters via the dog-house and the molten glass flows from the dog-house near-wall to the opposite end-wall. The firing ports are located along the sides of the furnace. There are four ports on each side, each port containing two fuel jets. The furnace is fired alternately from either side to give more uniform heat flux to the glass and to make the regeneration possible. The combustion products pass through regenerators which are used to preheat the combustion air before entering the furnace to produce higher temperatures and heat flux to the glass. Waste ports opposite burners working as outlet ports are demanded by the reversing operating conditions. Heavy oil is burned with excess of air. The roof furnace and side walls are refractory lined.

3. The physical modelling

The present modelling problem in its entirety has two distinct parts: the simulation of the combustion chamber and the glass tank. The authors have treated these separately, with the aid of different numerical solution procedures. The simulation of the whole furnace is a hybrid treatment involving the two codes.

3.1. Combustion chamber

The governing transport equations for the mean motion of a turbulent three-dimensional flow were applied in their cartesian coordinate form.

3.1.1. Mean flow equations

The time-averaged equations for the conservation of momentum are in compact tensor notation, as follows:

$$\frac{\partial}{\partial x_j}\left(\bar{\rho}\bar{u}_j\bar{u}_i + \bar{p}\,\delta_{ij} - \mu\left[\frac{\partial \bar{u}_i}{\partial x_j} + \frac{\partial \bar{u}_j}{\partial x_i} - \frac{2}{3}\frac{\partial \bar{u}_k}{\partial x_k}\delta_{ij}\right]\right) + (\bar{\rho} - \rho_{ref})g_i + \frac{\partial}{\partial_{x_j}}(\bar{\rho}\,\overline{u_j' u_i'}) = 0 \quad (1)$$

where u_i is the velocity component in the direction of coordinate x_i, ρ is density and ρ_{ref} a reference value, g_i is the magnitude of the gravitational acceleration in the i direction, p is pressure, μ is the laminar viscosity, and the operator δ_{ij} is unity for $i = j$ and zero when $i \neq j$.

The equation for the conservation of energy may be expressed as:

$$\frac{\partial}{\partial_{x_j}}(\bar{\rho}\bar{u}_j\tilde{h}) - \frac{\partial}{\partial_{x_j}}\left(\Gamma_h \frac{\partial \tilde{h}}{\partial_{x_j}}\right) + \frac{\partial}{x_j}(\bar{\rho}\,\overline{u_j'\tilde{h}'}) - \bar{S} = 0 \quad (2)$$

where $\tilde{h}$ represents stagnation enthalpy, Γ_h is equal to the fluid thermal conductivity divided by its constant-pressure specific heat, and $\bar{S}$ is a source term defined by:

$$\bar{S} = \bar{Q}_{rad} + \text{small terms} \quad (3)$$

where $\bar{Q}_{rad}$ is the net volumetric heat gain due to thermal radiation.

In addition to eqns (1–2) we must also include the equation of mass continuity:

$$\frac{\partial}{\partial x_j}(\bar{\rho}\bar{u}_j) = 0 \quad (4)$$

3.1.2. Turbulence model

The 'two-equation' model,[15] in which equations for the kinetic energy of turbulence, k, and its dissipation rate, ε, are solved, was considered appropriate. The correlations in eqn (1) are expressed, in analogy with laminar flow,[16] as:

$$-(\bar{\rho}\,\overline{u_j' u_i'}) = \mu_t\left(\frac{\partial \bar{u}_i}{\partial x_j} + \frac{\partial \bar{u}_j}{\partial x_i} - \frac{2}{3}\frac{\partial \bar{u}_k}{\partial x_k}\delta_{ij}\right) \quad . \quad (5)$$

where μ_t is a 'turbulent' viscosity that may be related to k and ε by dimensional arguments:

$$\mu_t = c_\mu \rho k^2/\varepsilon \quad . \quad (6)$$

where C_μ is a constant of the model. The turbulent exchange coefficient, $\Gamma_{\phi,t}$, for any variable, ϕ, may be expressed as:

$$\Gamma_{\phi,t} = \mu_t/\sigma_{\phi,t} \quad . \quad (7)$$

where $\sigma_{\phi,t}$ is a turbulent Prandtl number of order unity. Turbulent transport correlations involving ϕ' are determined from the Boussinesq approximation:

$$(\bar{\rho}\,\overline{u_i'\phi_i'}) = \Gamma_{\phi,t}\overline{\partial\phi/\partial x_i} \quad . \quad (8)$$

The differential equations for k and ε that the authors have solved are:

$$\frac{\partial}{\partial x_j}(\bar{\rho}\bar{u}_j k) - \frac{\partial}{\partial x_j}\left(\Gamma_k \frac{\partial k}{\partial x_j}\right) - \mu_t \frac{\partial \bar{u}_i}{\partial x_j}\left(\frac{\partial \bar{u}_i}{\partial x_j} + \frac{\partial \bar{u}_j}{\partial x_i}\right) + \bar{\rho}\varepsilon = 0 \quad . \quad (9)$$

and

$$\frac{\partial}{\partial x_j}(\bar{\rho}\bar{u}_j \varepsilon) - \frac{\partial}{\partial x_j}\left(\Gamma_\varepsilon \frac{\partial \varepsilon}{\partial x_j}\right) - C_1 \frac{\varepsilon}{k}\mu_t \frac{\partial \bar{u}_i}{\partial x_j}\left(\frac{\partial \bar{u}_i}{\partial x_j} + \frac{\partial \bar{u}_j}{\partial x_i}\right) + C_2 \bar{\rho}\frac{\varepsilon^2}{k} = 0 \quad . \quad (10)$$

where C_1 and C_2 are further constants and Γ_k and Γ_ε are determined via eqn (7).

The model constants used at present are well established in many previous furnace applications (see refs 5 and 17).

3.1.3. Combustion model

The combustion model is based on the ideal single step and fast reaction between the gaseous fuel and oxidant, assumed to combine in stoichiometric proportion. Equal effective turbulent mass diffusion coefficients for the fuel and oxidant and an instantaneous reaction were also assumed (see refs 18 and 19). As a consequence of these assumptions the flame thermodynamic state becomes related to a single passive scalar:

$$\phi = s m_{fu} - m_{ox} \quad . \quad (11)$$

where s is the stoichiometric oxygen required by mass, and m_{fu} and m_{ox} are the fuel and oxidant mass fractions.

The mixture fraction, f, is related to this quantity by:

$$f = (\phi - \phi_o)/(\phi_1 - \phi_0) \quad . \quad (12)$$

where the subcripts 1 and 0 designate the fuel- and oxidant-bearing streams. Furthermore, the authors have assumed that the chemical kinetic rate is fast with respect to the turbulent transport rate; then fuel and oxidant cannot co-exist, so $m_{fu} = 0$ for $m_{ox} \geqslant 0$ and $m_{ox} = 0$ for $m_{fu} \geqslant 0$, and the concentrations m_{fu} and m_{ox} are related linearly to f through eqns (11) and (12).

The transport equation for the mixture fraction, f, is given by:

$$\frac{\partial}{\partial x_j}(\bar{\rho}\bar{u}_j\bar{f}) - \frac{\partial}{\partial x_j}\left(\Gamma_f \frac{\partial \bar{f}}{\partial x_j}\right) = 0 \quad . \quad (13)$$

The above modelling, it may be noted, presumes a stationary thin flame envelope. The fluctuating nature of the turbulent reaction is more usually accommodated through a modelled equation for the variance of the mixture fraction fluctuations.[20]

The authors have adopted a statistical approach to describe the temporal nature of the mixture fraction fluctuations. The time-averaged value of any property, ϕ, solely dependent on f can then be determined from:

$$\bar{\phi} = \int_0^1 \phi(f) P(f)\,\mathrm{d}f \quad . \quad (14)$$

In the present work the authors have assumed the 'clipped normal' probability density function,[21] which is characterised by just two parameters, f, and the mean square of the f fluctuations, g:

$$g = \overline{(f - \bar{f})^2} \quad . \quad (15)$$

A modelled transport equation has been derived[19] for g which runs:

$$\frac{\partial}{\partial x_j}(\bar{\rho}\bar{u}_j g) - \frac{\partial}{\partial x_j}\left(\Gamma_g \frac{\partial g}{\partial x_j}\right) - C_{g1}\mu_t\left(\frac{\partial \bar{f}}{\partial x_j}\frac{\partial \bar{f}}{\partial x_j}\right) + \frac{C_{g2}}{k}\bar{\rho}\varepsilon g = 0 \quad (16)$$

where C_{g1} and C_{g2} are additional adjustable parameters.

As radiation plays a dominant role in the heat transfer process inside industrial furnaces, a simple and economical model for oil-fired furnaces was used in which it was assumed that the oil spray evaporates instantaneously.

3.1.4. Thermodynamic relations

The mixture specific enthalpy may be defined by:

$$h = \sum_{allj} m_j \int_0^T C_{pj}(T)\,\mathrm{d}T + m_{fu}H. \quad . \quad (17)$$

where C_{pj} is the constant-pressure specific heat of a species j.

Density was determined from the equation of state:

$$\rho = p \Big/ \left(RT \sum_{allj} m_j/M_j\right) \quad . \quad (18)$$

where p is pressure, R is the universal gas constant, and M_j is the molecular weight of species j. Since the m_j's, as well as T, are all functions of f, the time-averaged density for use in the mean flow equations was again determined from eqn (14).

(continued on

3.1.5. Soot model

The distinctive feature of oil-fired flames is their significant soot content. The proportion of total carbon content of the fuel which converts to soot is too small to influence significantly overall flame heat release distribution. Rather, soot is of concern because its presence greatly augments the radiation heat transfer and because it is a pollutant. Most reasonably operated and maintained modern burners ensure complete combustion of soot. So the primary function of the soot model will be good characterising of the optical behaviour of the flame. The soot content of heavy oil flames is so great that those of industrial dimensions approach the black body limit. In consequence, the accurate prediction of local soot concentration is not a prerequisite for good calculation of radiation transfer. This is indeed fortunate since the mechanisms of soot formation are far from being established even in the simplest laboratory flames.[22]

A simple global expression similar to that used by Khan and Greeves[23] was chosen to characterise soot production:

$$P_{s+} = C_f P_{fu} \phi^n \exp(-E/RT_g) \quad . \quad . \quad . \quad (19a)$$

C_f is a function which ideally depends on an easily definable fuel property such as the C/H ratio. The work of Abbas *et al*[24] has simply tuned it to flame data and these authors have found that a value of about 0.01 is appropriate. Although the work of Khan and Greeves[23] was carried out in connection with diesel engines, Abbas *et al*[24] found that their values of 3 and 40 200 cal/mol for n and E are useful. Soot production is essentially zero for equivalence ratios ϕ, less than that corresponding to the incipient sooting limit[25] and for ϕ in excess of a value corresponding roughly to the upper flammability limit. Following Khan and Greeves[23] the upper and lower limits have been set to two and eight respectively.

In one sense the determination of the soot-burning rate poses a much less demanding modelling problem, since the particle sizes are also so small that near-particle diffusion cannot possibly be controlling; rather, the combustion rate will be controlled by the rate of mixing of the particle-bearing vortices with adjacent oxygen-bearing material. A straightforward method of estimating this rate has been proposed by Magnussen and Hjertager,[26] who, following conventional turbulence concepts,[27] presume that the mixing rate is proportional to the magnitude of the time mean soot concentration, m_s, and the time-scale of the large scale turbulence motion ε/k. Their expression for the soot consumption rate is:

$$P_{s-} = A\bar{m}_s(\varepsilon/k)\rho \quad . \quad . \quad . \quad . \quad . \quad (19b)$$

where A is a model constant assigned the value four based on numerical experimentation. This relation will not be satisfactory in regions where the reaction rate is limited by oxygen deficiency, in which case Magnussen and Hjertager[26] propose:

$$P_{s-} = A\left(\frac{\bar{m}_{ox}}{\bar{m}_s s_s + \bar{m}_{fu} s_{fu}}\right)\bar{m}_s\left(\frac{\varepsilon}{k}\right)\rho \, . \quad . \quad . \quad (19c)$$

where s_s and s_{fu} are the soot and fuel stoichiometric ratios. The alternative that gives the smallest reaction rate is to be used.

Eqns (19) were used as the source term ($\bar{S}_s = P_{s+} - P_{s-}$) of the transport equation of soot mass concentration which runs:

$$\frac{\partial}{\partial x_i}(\bar{\rho}\bar{u}_i\bar{m}_s) - \frac{\partial}{\partial x_i}\left(\Gamma_s \frac{\partial \bar{m}_s}{\partial x_i}\right) - \bar{S}_s = 0 \quad . \quad . \quad (20)$$

3.1.6. Radiation model

The 'discrete transfer' radiation prediction procedure of Lockwood and Shah[28] has been utilised in this study. This method combines ease of use, economy and flexibility of application. This last feature is of particular importance in the real world of geometrically intricate combustion chambers. The claimed advantages of the method have now survived the rigours of several industrial applications, see refs 4 and 29, for example.

The 'discrete transfer' method is founded on a direct solution of the radiation transfer equation for a direction which runs:

$$\frac{\mathrm{d}I}{\mathrm{d}s} = (k_g + k_s)\left(\frac{E}{\pi} - I\right) \quad . \quad . \quad . \quad . \quad (21)$$

where I is the radiation intensity in a Ω direction, s is the distance in that direction, $E = \sigma T_g^4$ is the black body emissive power, and k_g and k_s are respectively the gas and soot absorption coefficients. The scattering terms do not appear, although they are easily accommodated, since the only particulate matter occurring in the present application is the soot particles, which are much too small to scatter significantly. Many radiation methods are based on the solution of the much more complex integro-differential equation which results when eqn (21) is rewritten for the whole solid angle, Ω. In the authors' opinion this is unsatisfactory since the numerical solution treatment of such an equation is necessarily very elaborate.

The authors have solved the much simpler eqn (21) within discretisation, $\mathrm{d}\Omega j$, of the whole solid angle, Ω, about selected directions, Ω. Assuming that E, k_g and k_s are constant over a finite distance increment δ_s, eqn (21) may be integrated to yield the simple recurrence relation:

$$I_{n+1} = \frac{E}{\pi}\{1 - \exp[-(k_g + k_s)\delta_s]\} + I_n \exp[-(k_g + k_s)\delta_s] \quad . \quad . \quad . \quad (22)$$

where n and $(n+1)$ are successive locations along Ω separated by the increment, δ_s. The relation is applied along the chosen Ω from known conditions at a point Q say (either guessed or pertaining to those of the previous iteration) on one wall to a point of impingement, P say, of the direction, Ω, on an opposite wall.

If the hemisphere above P is discretised into sub-angles, $\mathrm{d}\Omega_r$, within which the intensity is considered to be uniform; the energy flux arriving at P is:

$$q_{+,P} = \int_{\pi} I_P \Omega \, \mathrm{d}\Omega = \sum_{allr} I_P, \Omega_{r\to r} \, \mathrm{d}\Omega_r \quad . \quad . \quad (23)$$

The wall boundary condition is:

$$q_{-,P} = (1 - \varepsilon_w)q_{+,P} + \varepsilon_w E_w \quad . \quad . \quad . \quad (24)$$

where $q_{-,P}$ is the energy leaving the wall at P, ε_w is the wall emissivity, and $E_w = \sigma T_w^4$ is the wall emissive power. The value of I_{n+1} at point Q, the initial value required

for the application of the recurrence relation, eqn (22), is $q_{-,P}/\pi$. The net radiation heat flux is:

$$q_P = q_{+,P} - q_{-,P} \quad . \quad . \quad . \quad . \quad . \quad (25)$$

The net heat gain or loss within a small control volume of the flow procedure is:

$$S_R = (I_{n+1} - I_n)\Omega \, d\Omega \, dA \quad . \quad . \quad . \quad . \quad (26)$$

where the locations n and $(n + 1)$ correspond to the 'entry' and 'exit' of a direction into and from a control volume, and δA is the cell area projected normal to Ω. The energy sources, S_R, are appended to the energy balance equation solved for by the flow code.

The gas absorption coefficient, k_g, is calculated from the 'two grey plus a clear gas' fit of Truelove.[30] Water vapour and carbon dioxide are the prime contributors to the gaseous radiation. The total gas emittance is expressed by:

$$\varepsilon_g = \sum_n a_{g,n}(T)[1 - \exp(-k_{g,n}(p_w + p_c)L] \quad . \quad (27a)$$

where the summation n is over the three gases of the assumed mixture, the $k_{g,n}$ are presumed constant with the temperature dependence of the emittance being accommodated in the weighting coefficients, $a_{g,n}$, p_w and p_c are the partial pressures of the water vapour and carbon dioxide and L is the path length. The values of $k_{g,n}$ and $a_{g,n}$ are tabulated in ref 30. The value of k_g required for these calculations is obtained from the pseudo grey approximation:

$$\varepsilon_g = 1 - \exp(-k_g L) \quad . \quad . \quad . \quad . \quad . \quad (27b)$$

which has worked well in many furnace heat transfer computations.

3.2. Glass tank

The governing transport equations of the three-dimensional laminar flow were applied in their cartesian co-ordinate form.

3.2.1. Governing equations

The conservation of momentum may be written, in tensor notation, as follows:

$$\frac{\partial}{\partial x_j}\left[\rho u_j u_i + p\,\delta_{ij} - \mu\left(\frac{\partial u_i}{\partial x_j} + \frac{\partial u_j}{\partial x_i} - \frac{2}{3}\frac{\partial u_k}{\partial x_k}\delta_{ij}\right)\right]$$

$$-\rho g_i \beta(T - T_o) = 0 \quad . \quad . \quad . \quad . \quad . \quad (28)$$

where β is the volumetric coefficient of thermal expansion, and T_o is a reference temperature. All the terms have meanings equal to those in eqn (1), except the last one which represents the buoyancy term. The energy equation used is:

$$\frac{\partial}{\partial x_j}(\rho u_j T) - \frac{\partial}{\partial x_j}\left(\Gamma_T \frac{\partial T}{\partial x_j}\right) - S_T = 0 \quad . \quad . \quad (29)$$

The continuity equation, also used, is the following one:

$$\frac{\partial}{\partial x_j}(\rho u_j) = 0 \quad . \quad . \quad . \quad . \quad . \quad . \quad (30)$$

The property values, varying with temperature, were calculated by special functions, as described below.

The dynamic viscosity was calculated by the Fulcher-Vogel-Tamman eqn:[31]

$$\mu = \exp\left(-A + \frac{B}{T - T_o}\right) \quad . \quad . \quad . \quad . \quad (31)$$

where A, B and T_o are constants calculated from ref 33.

The density was calculated from the following eqn:[31]

$$\rho = \rho_o[1 - \beta(T - T_o)] \quad . \quad . \quad . \quad . \quad (32)$$

where ρ_o is the density of the molten glass at the temperature T_o.

The radiation transfer was handled by the Rosseland (optically thick) approximation, which results in appropriately augmented thermal conductivities in the energy balance equation. From Tooley,[32] the thermal conductivity was given by:

$$K_{eff} = (C_1)_k T^3 \quad . \quad . \quad . \quad . \quad . \quad . \quad (33)$$

where $(C_1)_k$ is a constant calculated from ref 33.

It was assumed from experimental observation that the batch region, which is a mixture of raw material (sand) and recycle glass, forms a thin layer covering the molten glass from the dog-house (batch inlet-door) until the second burner. It was also assumed that the batch temperature varies linearly between the inlet batch temperature and the melting temperature of the batch.

4. The numerical solution procedure

4.1. Preliminary consideration

The combustion chamber and the glass tank were simulated separately by different numerical solution procedures used as a hybrid treatment to simulate the whole furnace.

Nearly all industrial furnaces are three-dimensional and show disparity of scales, in that most of the combustion takes place within a volume surrounding the burner, which occupies only a small proportion of total furnace volume but requires a disproportionately large proportion of the total computational grid.

To avoid excessive memory requirement, in the present study the combustion chamber is assumed to consist of slices. Each slice is contained between the midway plane of one inlet-port and the midway plane between this inlet-port and the neighbouring one. As shown in Fig. 1, there are four inlet-ports with two burners in each one, which makes eight slices to simulate the whole combustion chamber.

In the work of Megahed[17] the combustion chamber was calculated in two slices, the first simulating the region over the molten glass and the second the region over the batch. However, in the present case the inlet conditions differ significantly from one port to another (see Table 1)

TABLE 1 Inlet conditions[33]

Port No (Fig. 1)	1	2	3	4
Total fuel flow (kg/h)	327	496	496	175
Total air flow (kg/h)	5480	8100	8680	3810
Excess air (%)	14	11	19	48
Fuel velocity (m/s)	0.505	0.765	0.765	0.27
Air velocity (m/s)	4.23	6.34	6.70	2.94

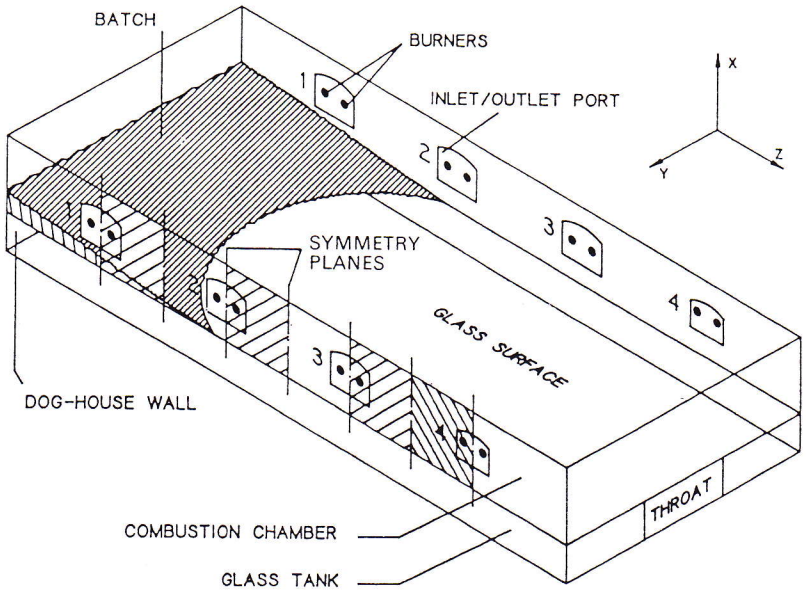

FIG. 1 Sketch of the furnace

and the overall performance of the combustion chamber was obtained by studying four slices (each one containing different inlet-ports).

Owing to the large period of time between the changes of side-firing in the furnace, the cycling nature of the firing process was neglected.

The glass tank predictions were made for its entire volume as particular refinement of the grid was not demanded.

4.2. Method of solution

The finite difference method used to solve the equations entails subdividing the combustion chamber and the tank into a number of finite volumes or 'cells'. Both solution algorithms are embodied in versions of the TEACH program[34] for three-dimensional recirculating flows. The convection terms were discretised by the hybrid central/upwind method.[35] The resultant difference equation has the form:

$$(a_P - S_P)\phi_P = \sum_n a_n\phi_n + S_o \quad . \quad . \quad . \quad . \quad (34)$$

where $a_P = \sum_n a_n$ and $\sum$ denotes summation over the six neighbouring nodes. One such equation exists for every scalar variable at every grid node. In the case of the velocities similar equations apply, but the control volumes are displaced such that they pass through the pressures driving the component in question, necessitating minor changes to the coefficient expressions.

In the combustion chamber predictions, the velocities and pressure are calculated by a variant of the SIMPLE algorithm described in ref 36. As presented there, this algorithm involves the solution of the momentum equations using the prevailing pressures, $\bar{p}^*$, to yield an intermediate velocity field denoted by $\bar{u}^*$; then velocity corrections are defined, linked to corresponding pressure corrections by relations of the form:

$$\bar{u}'_{j,b} = D^u_n(\bar{p}'_n - \bar{p}'_P) \quad . \quad . \quad . \quad . \quad . \quad (35)$$

where $D^u_n = \partial u_{j,b}/\partial(p_n - p_P)$ is evaluated from the relevant momentum equation. Eqn (35) is substituted into the integrated form of the continuity equation to give:

$$a_P\bar{p}' = \sum_n a_n\bar{p}' + S_o \quad . \quad . \quad . \quad . \quad . \quad (36)$$

from which $\bar{p}'$, and hence $\bar{u}'$, is determined. Eqn (36) may be recognised as a form of Poisson equation for the pressure correction, in which $S_o = -\sum_b \dot{m}_b$ is the local continuity imbalance of the momentum-based $\bar{u}^*_j$ velocities. Following solution of this equation, the corrections are applied by setting $\bar{u}_j = \bar{u}^*_j + \bar{u}'_j$, $\bar{p} = \bar{p}^* + \bar{p}'$, and the entire procedure is repeated until momentum and continuity are both satisfied. The calculations of the remaining dependent variables, as well as the updating of the thermodynamic and transport properties, are incorporated into the above sequence.

In the tank flow predictions, the velocities and pressure are calculated by a variant of the PISO algorithm presented by Issa.[13]

Using operator notation, eqn (34) becomes:

$$A^{Ui}_P U_i = H(U_i) - \Delta_i p + S^{Ui}_P \quad . \quad . \quad . \quad (37a)$$

$$H(U_i) = \sum A^{Ui}_k U_k \quad . \quad . \quad . \quad . \quad . \quad (37b)$$

and Δ_i is the discretised divergence. Denoting iteration levels with 'n' and successive levels of splitting (intermediate values) with '*', '**' and '***', the algorithm for the hydronynamics equations is:

Predictor stage: with a guessed value of pressure (or using the value from the previous iteration), p^n, the first intermediate velocities are calculated by:

$$A^{Ui}_P U^*_i = H^n(U^*_i) - \Delta_i p^n + S^{Ui}_P \quad . \quad . \quad . \quad (38)$$

First corrector stage. The first pressure increment is calculated by:

$$\Delta_i\left[\frac{1}{A^{U_i}_p}\Delta_i(p^* - p^n)\right] = \Delta_i(U^*_i) \quad . \quad . \quad . \quad (39)$$

and the first velocity correction is given by the solution of the following explicit equation:

$$U^{**}_i = U^*_i - \frac{1}{A^{U_i}_P}\Delta_i(p^* - p^n) \quad . \quad . \quad . \quad . \quad (40)$$

Second corrector stage: The second pressure increment

$$\Delta_i\left[\frac{1}{A_P^{U_i}}\Delta_i(p^{**}-p^*)\right]=\Delta_i\left[\frac{1}{A_P^{U_i}}H^n(U_i^{**}-U_i^*)\right] \quad (41)$$

$$U_i^{***}=U_i^{**}+\frac{1}{A_p^{U_i}}[H^n(U_i^{**}-U_i^*)-\Delta_i(p^{**}-p^*)] \quad (42)$$

The fields U_i^{***} and p^{**} are taken as the new iteration level ones. This is the original algorithm,[13] and the temperature is calculated after the second corrector stage.

In the present study, the temperature calculation was incorporated into the algorithm, as the source term of the V velocity component depends on it:

$$S_V=\rho_o\beta(T-T_o)g\,\mathrm{d}V \quad (43)$$

The incorporation was made as follows:

- After the first corrector stage the temperature equation was solved.
- A new source term, eqn (43), was then calculated for the V velocity component. As a consequence of this calculation, eqns (41) and (42) became:

$$\Delta_i\left[\frac{1}{A_P^{U_i}}\Delta_i(p^{**}-p^*)\right]=\Delta_i\frac{1}{A_P^{U_i}}[H^n(U_i^{**}-U_i^*)+(S_{U_i}^*-S_{U_i}^n)] \quad (44)$$

$$U_i^{***}=U_i^{**}+\frac{1}{A_P^{U_i}}[H^n(U_i^{**}-U_i^*)-\Delta_i(p^{**}-p^*)+(S_{U_i}^*-S_{U_i}^n)] \quad (45)$$

- The temperature equation was then solved again, and a new iteration was restarted.

The solution of the individual equation sets was obtained by a form of Gauss-Seidel line-by-line iteration, in both sub-models.

5. Presentation and discussion of results

5.1. Some computational details

The present prediction procedure was applied for the solution of the process in a full-scale industrial glass furnace with real operating conditions. The daily production of glass, or the throughput, is 100 tonnes. As described earlier, the furnace contains four firing ports. Total mass flow of fuel and air at each port can be found in Table 1.

The fuel is injected at 393 K and the air is preheated to be injected at 1273 K. The fuel composition is 86% of carbon and 14% of hydrogen. The inlet axial velocities of fuel and air can be found in Table 1. The radial and tangential velocities were set to zero owing to the absence of swirl. The kinetic energy of turbulence at the inlet is assumed to be 0.3% of the kinetic energy of the mean flow and its dissipation rate, ε, is calculated from the relation:

$$\varepsilon_{in}=\frac{6.0K_{in}^{1.5}}{l}$$

where l is a characteristic length scale. The glass temperature distribution calculated by the glass tank sub-model was used to predict the furnace combustion chamber.

Part of the upper surface of the molten glass is covered by a batch blanket. Close to this solid surface, the tangential velocity is set to zero owing to the non-slipping interface fluid-solid condition. In the remaining part of the referred surface the velocity is calculated from a vanishing shear-stress condition. A given parabolic profile was used for both inlet and outlet velocities.[3] A given heat flux, calculated by the combustion chamber sub-model, was used to predict the glass tank operating conditions.

Overall heat transfer coefficients were calculated based upon the thickness of the building material and external cooling conditions given by ref 33. These values vary from 1.9 to 7.1 W/(m^{2}K).

For the combustion chamber predictions, a numerical grid comprising 14 × 10 × 14 grid nodes in the x, y and z coordinate directions respectively was used, simulating each half-port slice of the furnace, while for the whole of the glass-tank predictions a 14 × 16 × 27 grid was used.

In radiation calculations for the combustion chamber, 16 rays were tracked from each boundary-cell (usually four or eight rays are used, see Carvalho[5] and Semiao,[6] for example), which augments considerably the time consumed per iteration, but convergence is achieved in a smaller number of iterations and the converged solution approximates much more closely to the furnace operating conditions.[28]

Calculations for the whole of the furnace were carried out by the following procedure:

1. A slice of the combustion chamber corresponding to one of the half-ports (Fig. 1) was predicted, assuming a distribution of glass surface temperature. The results obtained were used as initial values to predict the remaining three half-ports slices of the combustion chamber. For the first run, 300 interations were needed (38 CPU hours in a MicroVax II) to achieve convergence (the results were considered converged when the normalised residuals of the equations were less than 5×10^{-3}). For the other runs, only 120 iterations (15 CPU hours) were needed.
2. With the fluxes to the glass, calculated from the previous runs, the whole glass tank was predicted, with the same convergence criteria, which takes 120 iterations (13 CPU hours in the same computer machine).
3. The temperature distribution of the glass surface was then used to repeat the whole process from 1.
4. The procedure was considered 'converged' when the glass surface temperatures and the fluxes to the glass did not vary more than 10% from one cycle to the next one.

At the end of the fourth cycle 'convergence' was achieved, which shows the strong relation between the two processes.

5.2. Discussion of results

Some general aspects of the model's predictions are illustrated in Figs. 2–10. Owing to the qualitative similarity of the combustion chamber results, only the third half-port slice predictions are presented here.

(continued on

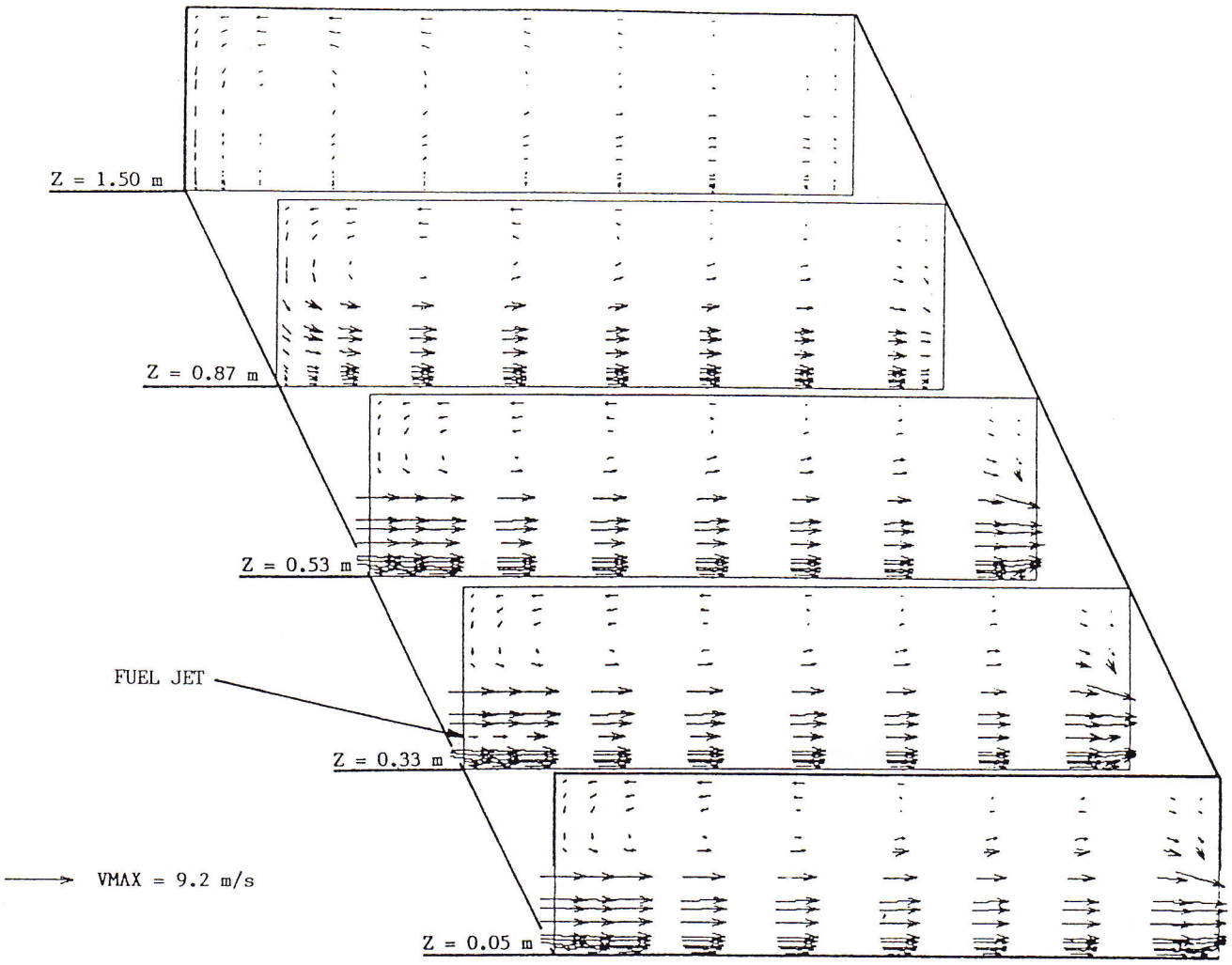

FIG. 2(a) Velocities on constant z planes for combustion chamber

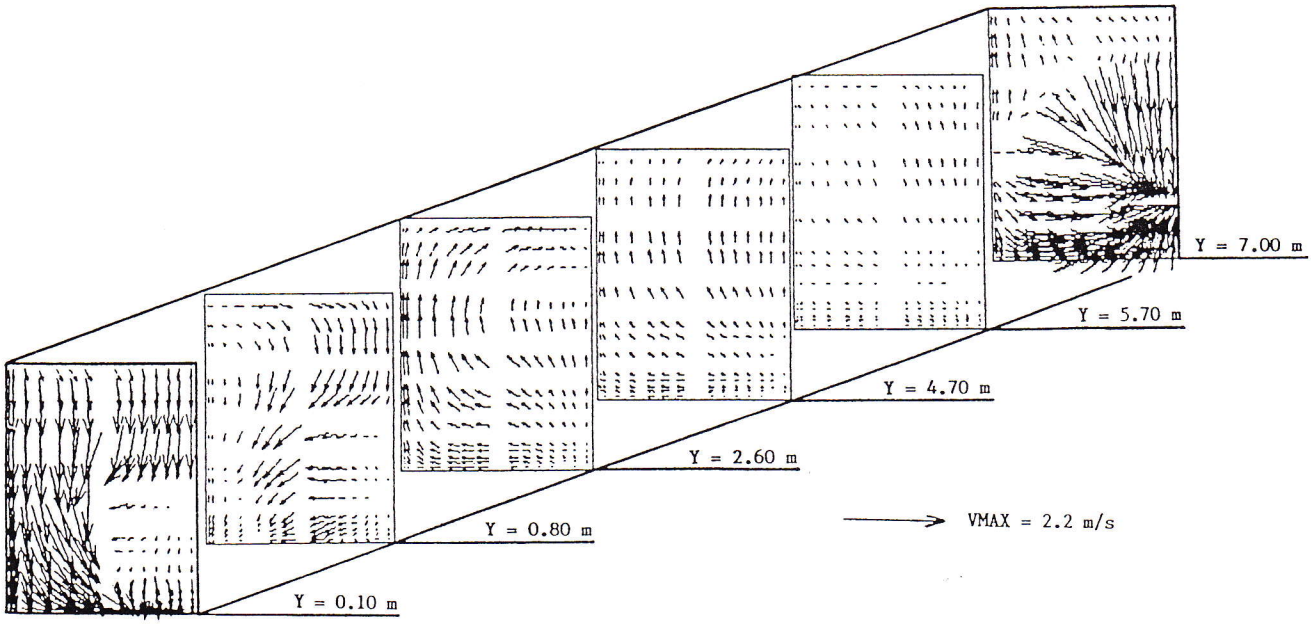

FIG. 2(b) Velocities on constant y planes for combustion chamber

5.2.1. Velocity

Fig. 2(*a*) shows predicted projections of velocity vectors on vertical planes normal to the inlet-port containing wall, while Fig. 2(*b*) shows the referred projection on vertical planes parallel to the referred wall. The first three planes ($z = 0.05$ m, $z = 0.33$ m and $z = 0.53$ m) in Fig. 2(*a*) contain the inlet- and outlet-ports and show that the flow is mainly a jet crossing the furnace from the inlet to

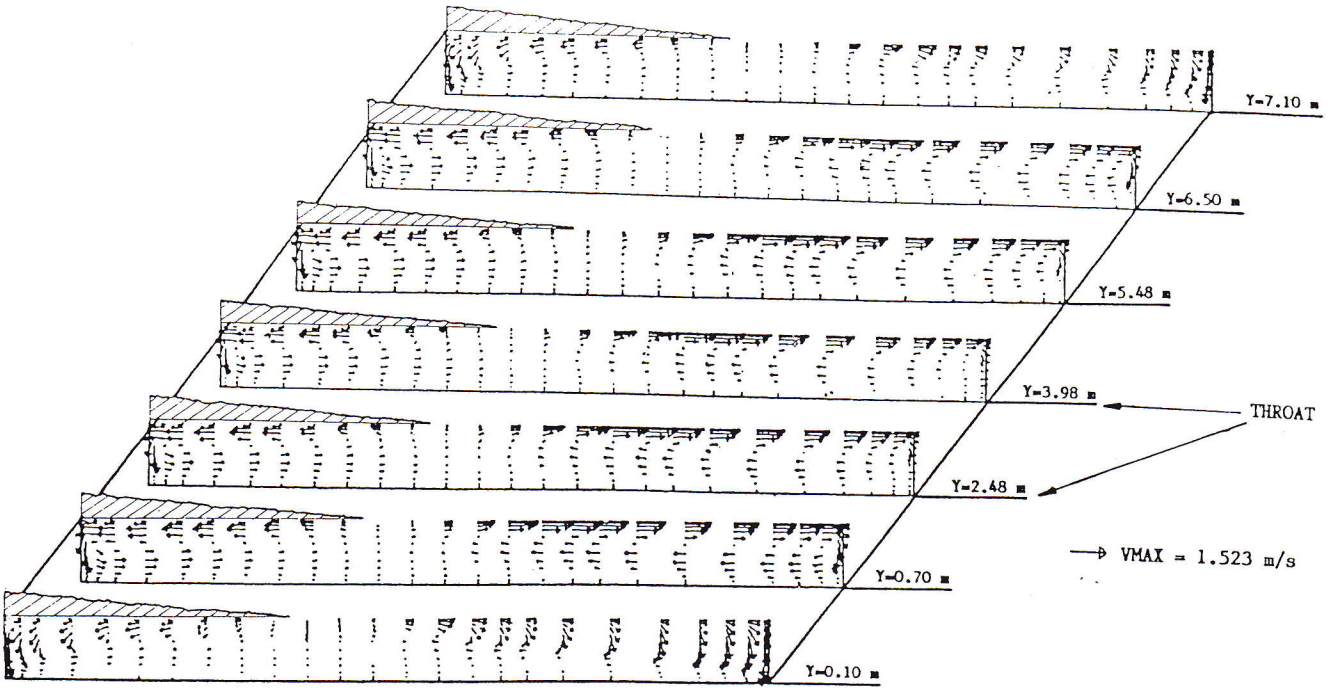

FIG. 3 Velocities on constant y *planes for glass tank*

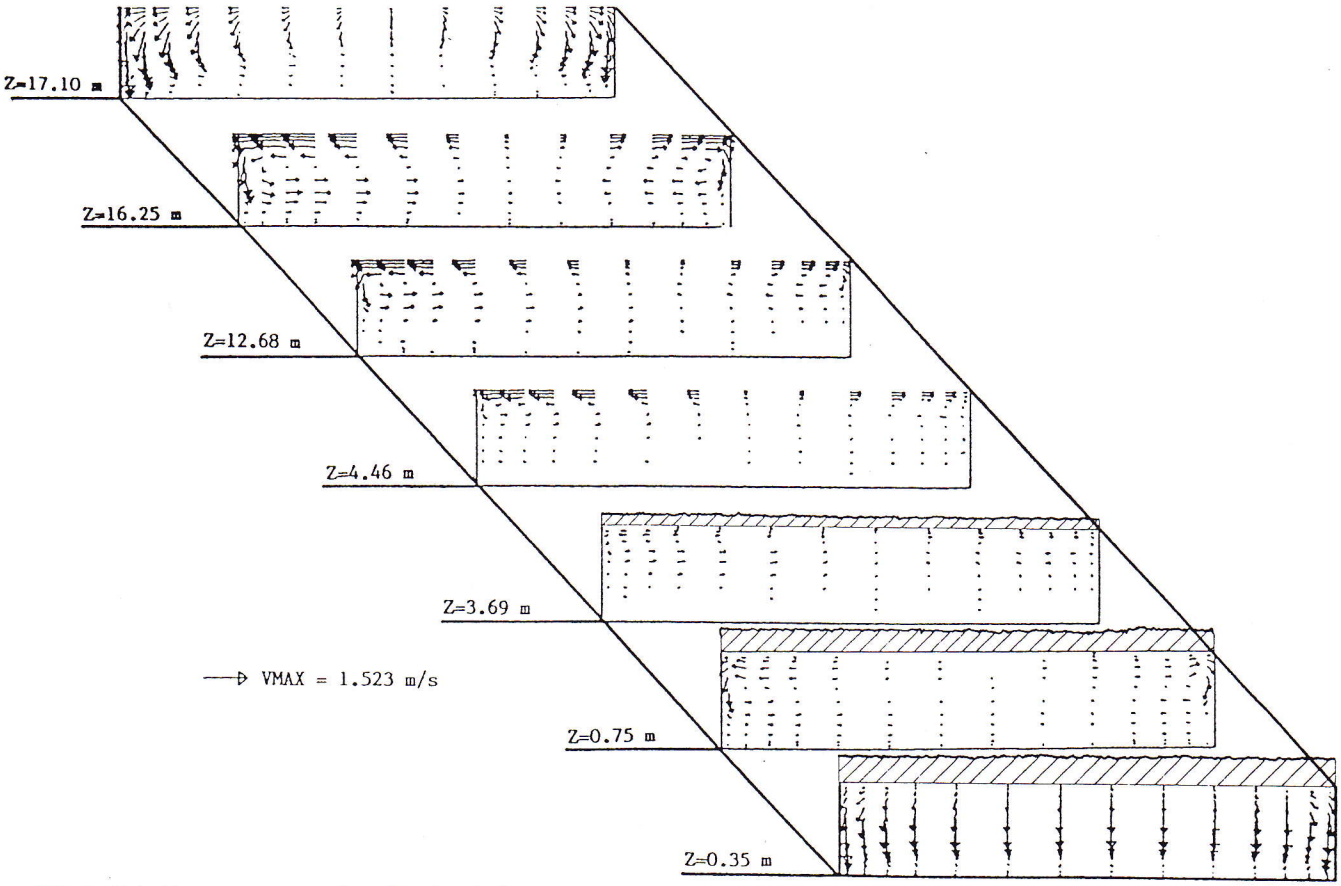

FIG. 4 Velocities on constant z *planes for glass tank*

the outlet-port. A recirculation zone can be found on the upper portion of the furnace and near the roof the main flow is inverted. This recirculation slightly directs the inlet jets towards the glass near the inlet-port as shown in the two first planes of Fig. 2(*b*). This figure also shows that the flow is strongly three-dimensional.

As regards the batch flow, Figs. 3 and 4 show respectively the predicted projections of the velocity on longitudinal and transversal vertical planes. The main flow pattern predicted by the model, shown in Fig. 3, is the anti-clockwise circulation next to the side wall for the left-hand half of the furnace, and a clockwise circulation in the remaining part of the furnace. The former is maintained by cold glass falling from the unstable layer

(*continued on p 152*)

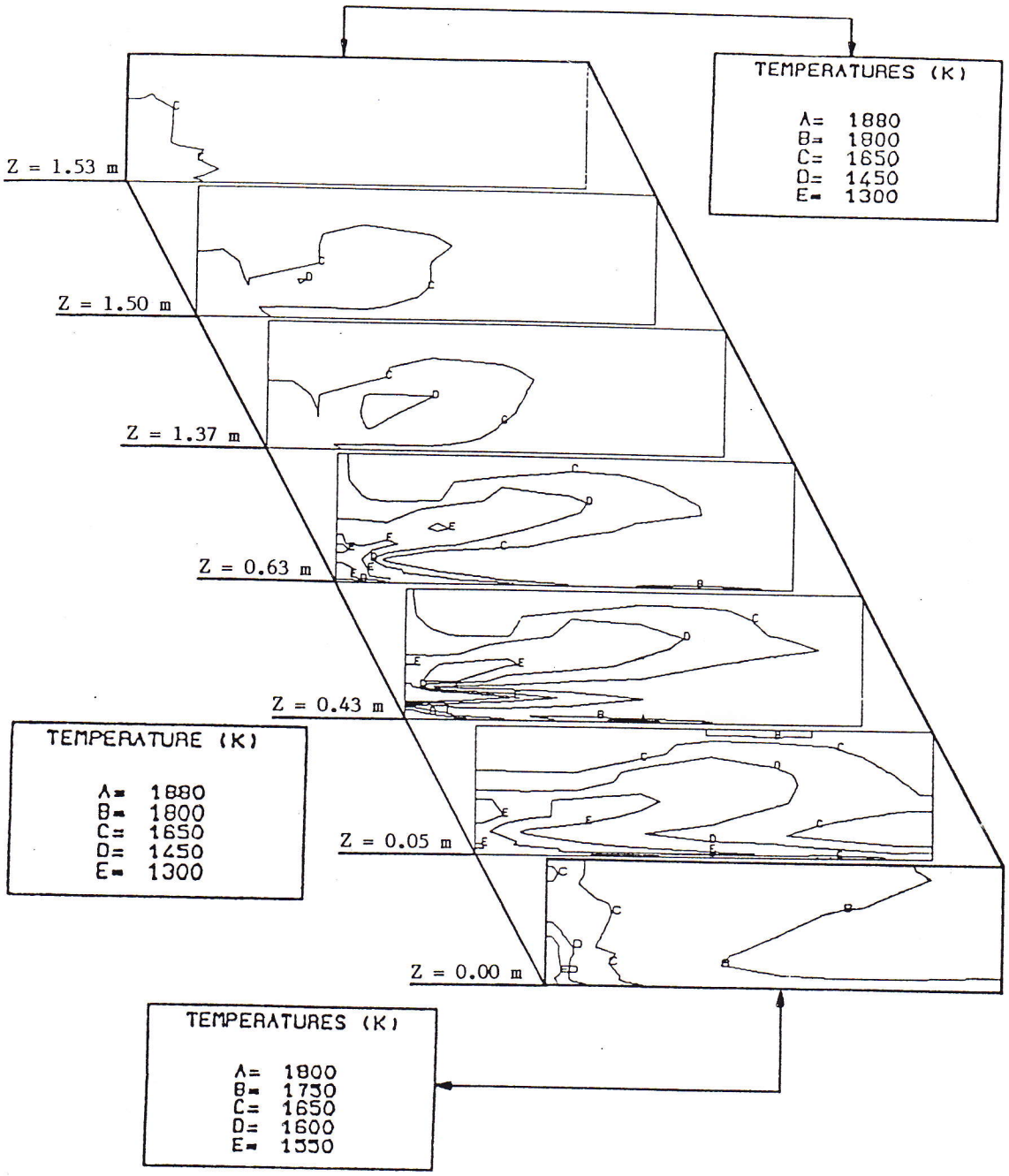

FIG. 5(a) Temperatures on constant z planes for combustion chamber

that exists below the batch crust. The hot glass is displaced towards the centre of the furnace by convection currents.

It should be noted that the circulating cells are stagnant so that the glass flowing through the system is confined to an extremely thin zone between the cells and to a very thin superficial layer on the right-hand cell which carries the glass through the throat. Against the daily production of 100 t of glass there are 700 t circulating inside the tank as calculated by the model. In practice, however, there will always be small disturbances to the system which will allow some glass to escape from the stagnant zones.

The linear velocities due to the pull are so small compared with those due to convection that the vector velocities leaving the batch and entering the throat cannot be shown on the same scale as that used in Fig. 3. Fig. 4 shows two recirculating cells in the region where there is no batch. These cells help to make the glass homogeneous, therefore improving its quality, and act as a source of the main longitudinal cells.

5.2.2. Temperature

Figs. 5(*a*) and (*b*), show the temperature distribution in the combustion chamber, in a similar arrangement of the velocity vectors. The first and the last planes on Figs. 5(*a*) and 5(*b*) represent respectively the symmetry planes and the inlet and outlet walls. In the reaction zone the temperature is higher than in the other zones with a maximum value of 1880 K. Outside the flame region the temperature is near homogeneous. Temperatures are higher below the horizontal plane containing the burner than above it. This is due to the upper recirculation zone

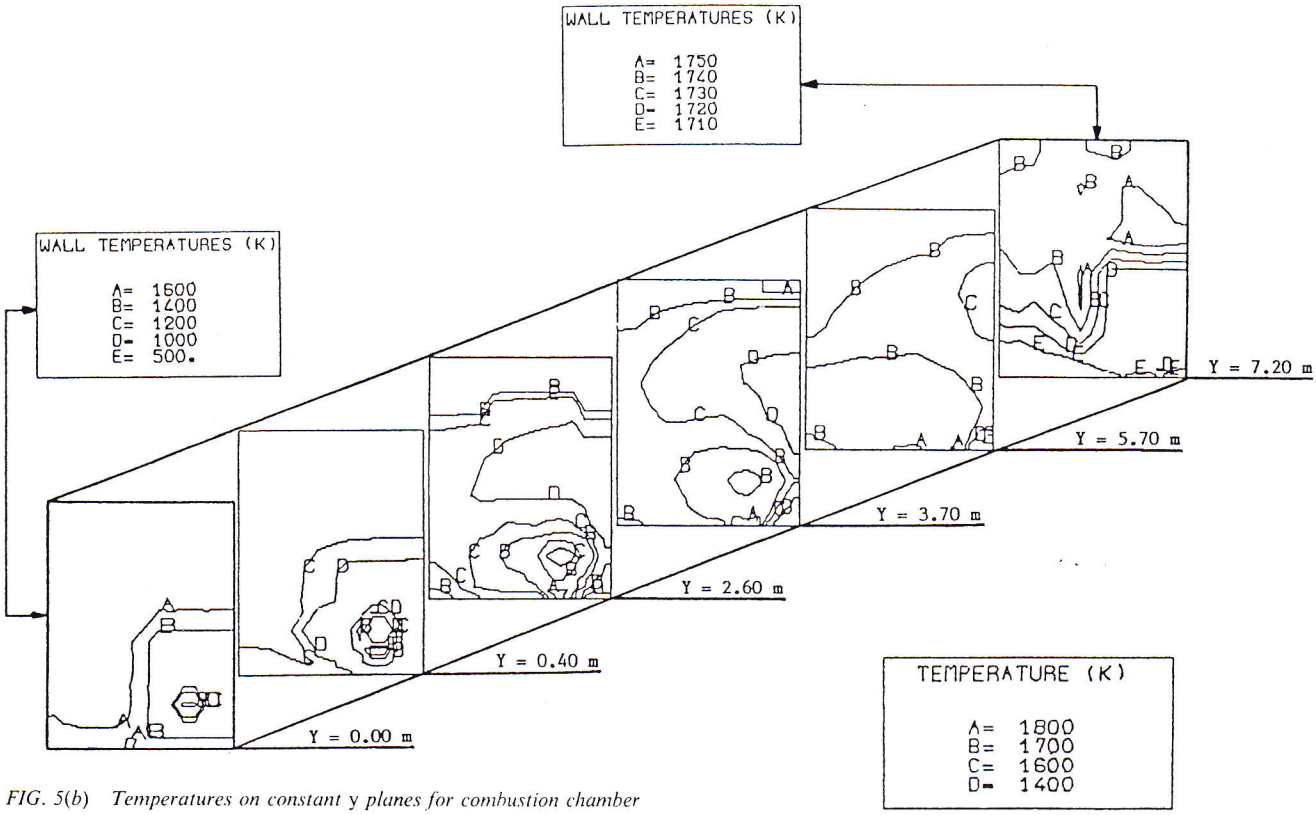

FIG. 5(b) Temperatures on constant y planes for combustion chamber

which slightly directs the flame towards the glass in the first metres after the injection.

In the tank zone longitudinal and transversal isothermal lines are shown (Figs. 6 and 7). These figures show that high temperature values and gradients appear near the hot-point (where the maximum value is 1670 K). The temperature decreases and becomes stratified as one moves towards the bottom of the tank. As described before, these temperature gradients are the driven forces of the glass flow (buoyancy forces).

5.2.3. Mixture fraction

Fig. 8 shows the mixture fraction distribution in vertical planes normal to the inlet-port containing wall. The predicted flame length (based on the definition of 'chemical length'—distance from the burner exit to the point of stoichiometric fuel concentration) was 6.8 m, which agrees well with the visual estimation of the flame length of 6.5 m.

Fig. 9 shows respectively the fuel, oxygen and carbon dioxide mass concentrations on the burner plane, which are related to the mixture fraction distribution as described in section 3.1.3. The main feature of these figures is the poor mixing pattern between oxygen and fuel in the first metres of the furnace. This is the result, mentioned above, of the upper recirculation which directs the fuel-jet to a poor oxygen content region. As a consequence there is a small amount of wasted unburned fuel at the outlet. A parametric study of the burner angle of inclination would be advisable. The carbon dioxide concentration is maximum where the reaction has taken place, as one would expect.

5.2.4. Soot concentration

The predicted contours of soot mass concentration are shown in Fig. 10. The maximum soot mass concentration value (5×10^{-2} kg/m^3) occurs in the burner axis in the middle of the furnace. The non-zero soot mass concentration should be noted at the outlet; this is an important result due to the pollutant nature of soot.

A strong similarity is observable between the contours of m_s and m_{fu}. This confirms the strong influence of the amount of insufficiently mixed fuel in regions of high temperature in the soot formation process, as expressed in the model used.

5.2.5. General results

Validation of furnace predictions against experimental data acquired in real-life operating furnaces is an important task. In spite of that, measurements are uncommon as they are obtained with difficulty, owing to high temperature and high corrosion levels occurring inside the furnaces.

A few values for outlet data are given in ref 33 and are compared with predicted values in Table 2.

TABLE 2 Data for outlet-port No 3

Variable	Experimental values[33]	Predicted values
Outlet velocity (m/s)	8.30	8.60
Outlet temperature (K)	1720	1710
Outlet CO_2, mass concentration	0.14	0.15
Outlet O_2, mass concentration	0.034	0.04

As can be seen, the predicted values do agree quite well with the very few experimental ones. In spite of the lack of good quantitative validation evidence, trends in the results show that the performance of this furnace is well characterised by the model. In the numerical treatment of this furnace some sources of inaccuracy may be present

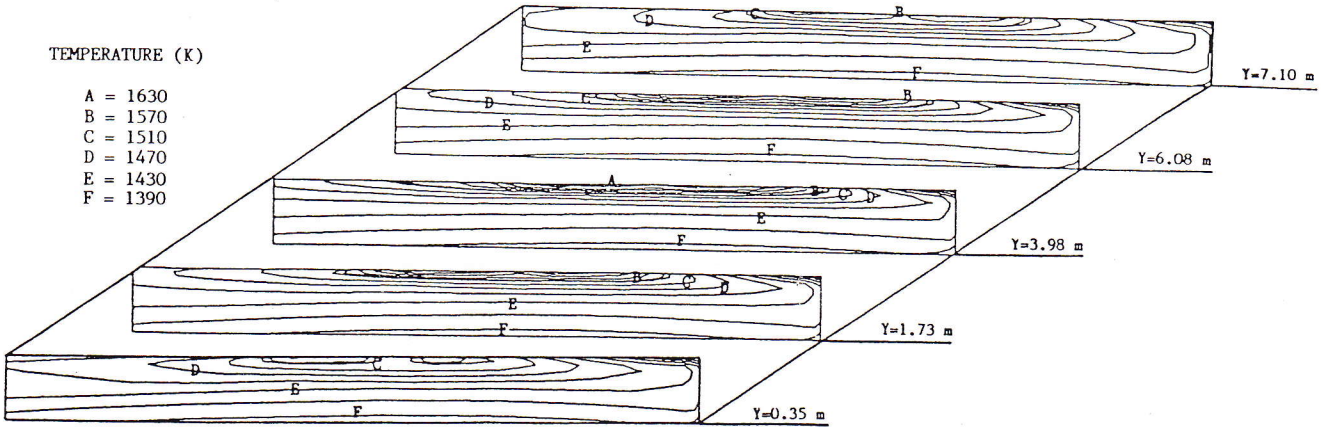

FIG. 6 Temperatures on constant y planes for glass tank

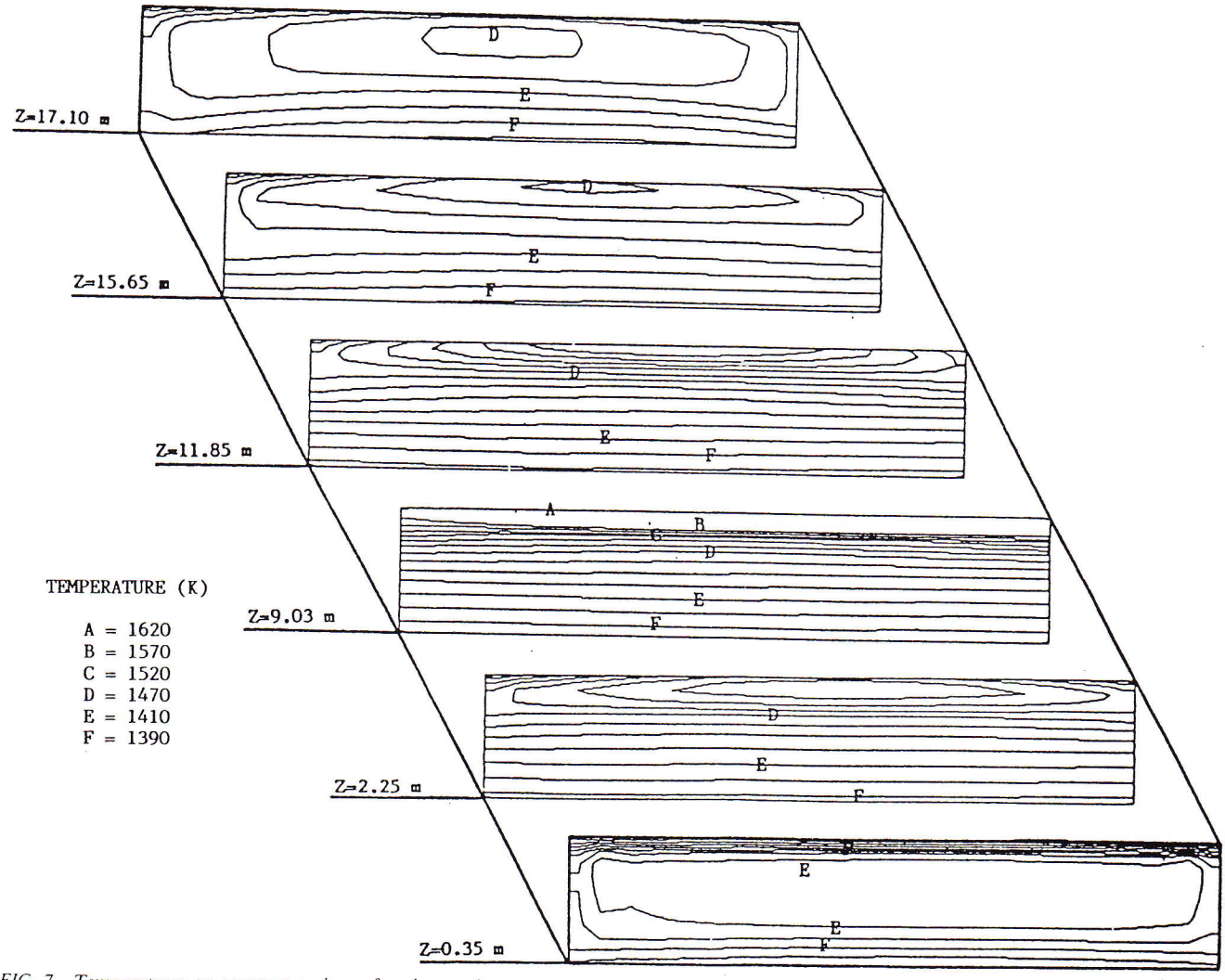

FIG. 7 Temperatures on constant z planes for glass tank

The interaction between two neighbouring flames is neglected. The application of the hybrid/central upwind scheme may lead to numerical diffusion. The sources of error, together with the simplicity of the turbulence and combustion models have proved to be, in the previous application,[8] minor. Indeed, the combustion chamber models used in this model are the same as those used by Carvalho *et al*,[8] where extensive validation of predictions against experimental data acquired in a real furnace were arises from the importance of radiation in large industrial furnaces.

6. Conclusions

The paper describes the application of a useful and general prediction procedure to a real-life industrial furnace. The authors suggest that the processes occurring in the combustion chamber and in the glass tank of an

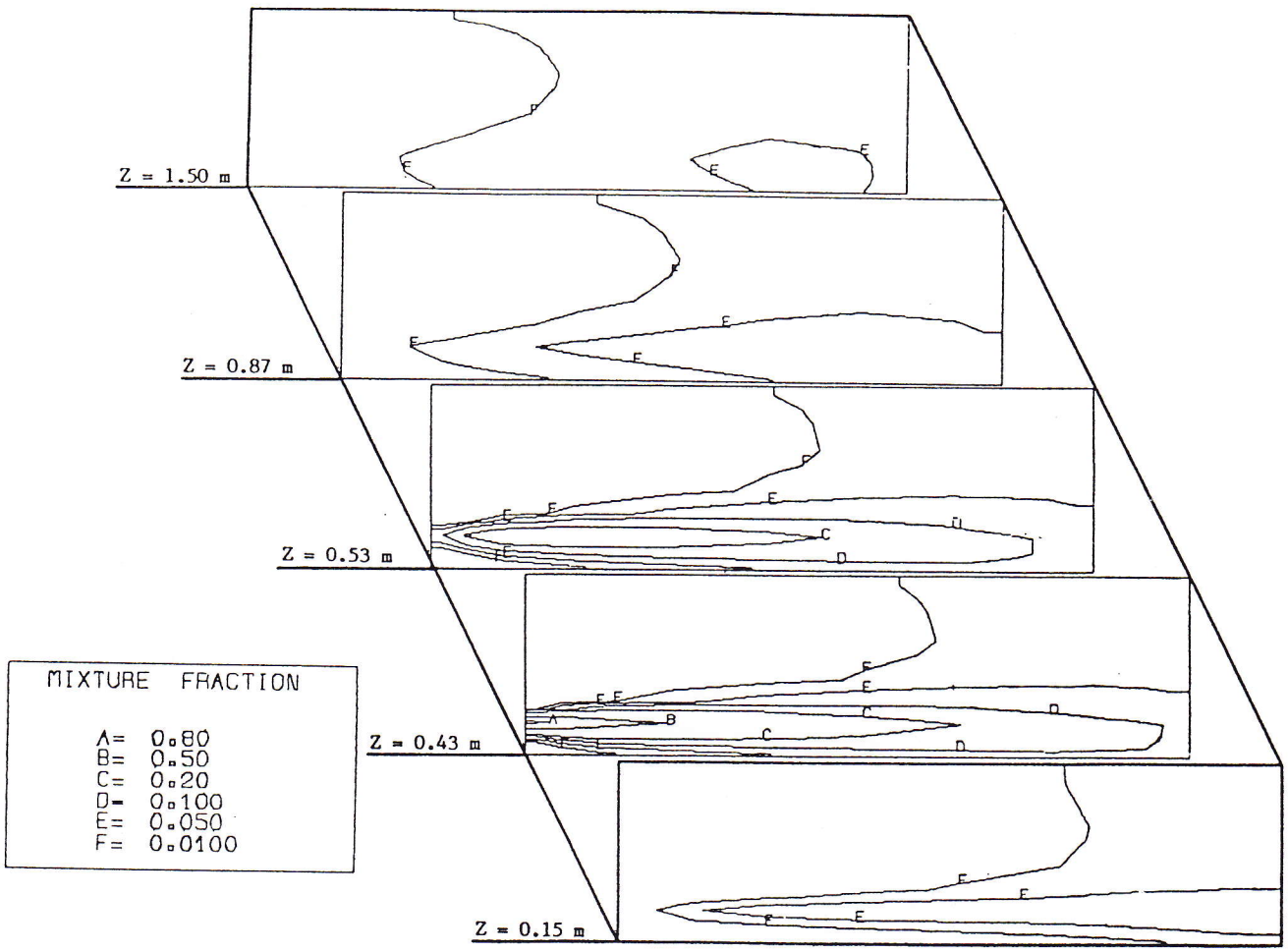

FIG. 8 Mixture fraction contours on constant z planes for combustion chamber

engineering accuracy at moderate low cost by numerical procedures. The modelling of all relevant physical and chemical processes, in both combustion chamber and glass tank, constitutes a major improvement to the previous treatment of the problem and, more importantly, provides the engineer with good estimates of all related parameters. There seems little question that prediction procedures of the present kind will prove to be a valuable tool for the furnace designer.

7. Acknowledgments

The authors wish to thank the COVINA Laboratories for theoretical advice. The final manuscript was completed with the help of Ms M Cristóvão, Ms S Valério and Mr R Ferreira.

8. References

1. CHEN T and GOODSON R E. Computation of three-dimensional temperature and convective flow profiles for an electric glass furnace. *Glass Tech*, 1972, **13**(6), 161–167.
2. SUZUKI J. Three-dimensional flow and temperature distributions in rectangular cavities. MSc thesis, University of Sheffield, 1976.
3. OLIVEIRA P J. Convecção natural: um estudo numérico. Aplicação ao escoamento do vidro num forno tanque. MSc thesis, University of Lisbon, 1986.
4. GOSMAN A D, LOCKWOOD F C, MEGAHED I E A and SHAH N G. The prediction of the flow reaction and heat transfer in the combustion chamber of a glass furnace. AIAA 18th meeting on *Aerospace sciences*,
5. CARVALHO M G. Computer simulation of a glass furnace. PhD thesis, University of London, 1983.
6. SEMIAO V S. Simulação numérica de uma fornalha industrial. MSc thesis, University of Lisbon, 1986.
7. CARVALHO M G, DURÃO D F G and PEREIRA J C. The prediction of the flow, reaction and heat transfer in an oxy-fuel glass furnace. *Int J Comput Aided Eng & Software*, 1987, **4**, 23–31.
8. CARVALHO M G, DURÃO D F G, HEITOR M V and MOREIRA A L. The flow and heat transfer characteristics of an industrial glass furnace. Internal Report, 1987, Dept of Mech Eng, Instituto Superior Técnico, Lisboa (to be published).
9. MCCONNELL R R and GOODSON R E. Modelling of glass furnace design for improved energy efficiency. *Glass Tech*, 1979, **20**(3).
10. MASE H and ODA K. Mathematical model of glass tank furnace with batch melting process. *J Non-Cryst Solids*, 1980, **38** and **39**, 807–812.
11. NOVAK J D. Application of combustion space energy calculations to commercial glass furnaces. *J Non-Cryst Solids*, 1980, **38** and **39**, 819–824.
12. CARVALHO M G and LOCKWOOD F C. Mathematical simulation of an end-port regenerative glass furnace. *Proc Inst Mech Eng*, 1985, **199** (No C2), 113–120.
13. ISSA R I. The solution of fluid flow equations operator splitting. Report No FS/82/15, Dept of Mech Eng, Imperial College, London, 1982.
14. ISSA R I, GOSMAN A D and WATKINS A P. The computation of compressible and incompressible recirculating flows by a non-iterative implicit scheme. Report No FS/83/8, Dept of Mech Eng, Imperial College, London, 1983.
15 LAUNDER B E and SPALDING D B. Mathematical models of turbulence. Academic Press, New York, 1972.
16. HINTZE J O. Turbulence. McGraw-Hill, New York, 1959.
17. MEGAHED I E A. The prediction of three-dimensional gas-fired combustion chamber flows. PhD thesis, University of London, 1978.

(continued on

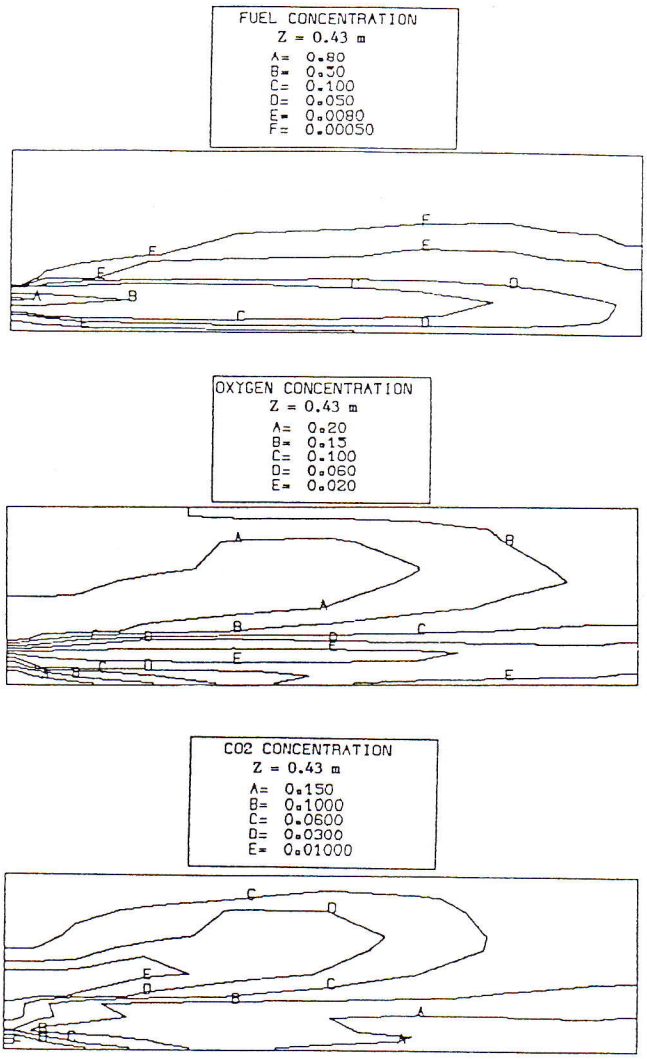

FIG. 9 Fuel, O_2 and CO_2 mass concentrations on plane z = 0.43 m for combustion chamber

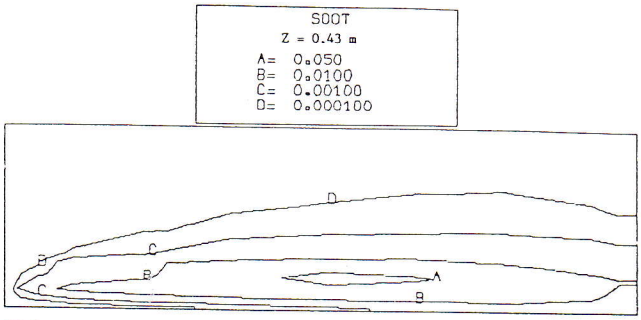

FIG. 10 Soot mass concentration on plane z = 0.43 m for combustion chamber

18. PUN W M and SPALDING D B. A procedure for predicting the velocity and temperature distributions in a confined steady, turbulent, gaseous diffusion flame. Proc Int Astronautical Federation meeting, Belgrade, 1967.
19. BILGER R W. Turbulent flows with non-premixed reactants, turbulent reacting flows. Topics in applied physics. Ed. Libby P A and Williams F A, Springer-Verlag, 1980.
20. SPALDING D B. Concentration fluctuations in a round turbulent free jet. *Chem Eng Sci*, 1971, **26,** 96.
21. LOCKWOOD F C and NAGUIB A S. The prediction of the fluctuations in the properties of free, round jet, turbulent diffusion flame. *Combust Flame*, 1975, **24** (No 1), 109.
22. WAGNER H G. Soot formation in combustion. 17th symp (int) on *Combustion*, Combustion Institute, 1978.
23. KHAN I M and GREEVES G. A method for calculating the formation and combustion of soot in diesel engines. Heat transfer in flames. Ed. Afgan and Beér, 1974, pp 391–402.
24. ABBAS A S, KOUSSA S S and LOCKWOOD F C. The prediction of a variety of heavy oil flames. Proc ASME winter annual meeting, spec sess on *Two-phase combustion liquid fuels*. Washington, Nov 1981.
25. GLASSMAN I and YACCARINO P. The temperature effect in sooting diffusion flames. 18th symp (int) on *Combustion*, Combustion Institute, 1981.
26. MAGNUSSEN B F and HJERTAGER B H. On mathematical modelling of turbulent combustion with special emphasis on soot formation and combustion. 16th symp (int) on *Combustion*, Combustion Institute, 1976.
27. TENNEKES H and LUMLEY J L. A first course in turbulence. MIT Press, Cambridge (USA), 1973.
28. LOCKWOOD F C and SHAH N G. A new radiation solution method for incorporation in general combustion prediction procedures. 18th symp (int) on *Combustion*, Combustion Institute, 1981.
29. CARVALHO M G, DURÃO D F G and LOCKWOOD F C. Computation of thermal radiation for gas turbine conditions. Symp on *Heat transfer and cooling in gas turbines*, AGARD/PEP, May 1985, Bergen, Norway, May 1985.
30. TRUELOVE J S. A mixed grey gas model for flame radiation. AERE Harwell Report No HL 76/3448/KE, 1976.
31. STANEK J. Electric melting of glass. Elsevier Scien Pubi Co. Amsterdam, Oxford and New York, 1977.
32. TOOLEY F V. The handbook of glass manufacture. Vol **I,** Books for Industry Inc, 1974.
33. Batch melting and furnace data. Report of COVINA Labs, Lisbon, Portugal.
34. GOSMAN A D, HUMPHREY J A C and VLACHOS N S. TEACH-3E: A general computer program for three-dimensional recirculating flows. Report CHT/76/10, Dept of Mech Eng, Imperial College, London.
35. SPALDING D B. A novel finite difference formulation for differential expressions involving both first and second derivatives. *Int J Num Methods Eng*, 1972, **4,** 557.
36. CARETTO L S, GOSMAN A D, PATANKAR S V and SPALDING D B. Two calculation procedures for steady, three-dimensional flows with recirculation. Proc of 3rd int conf on *Numerical methods in fluid dynamics*. Springer-Verlag, New York, 1972, p 60.

(Paper received March 1987)